ACS OMEGA

Article

Cite This: ACS Omega 2018, 3, 3805−3812

Colorimetric Immunosensor by Aggregation of Photochemically Functionalized Gold Nanoparticles

Marzia Iarossi,[†,∥] Chiara Schiattarella,[†,‡] Ilaria Rea,[‡] Luca De Stefano,[‡] Rosalba Fittipaldi,[§] Antonio Vecchione,[§] Raffaele Velotta,*[,†] and Bartolomeo Della Ventura[†]

[†]Department of Physics "E. Pancini", Università di Napoli "Federico II", Via Cintia, 26 Ed. 6, 80126 Napoli, Italy

[‡]National Research Council, Institute for Microelectronics and Microsystems, Unit of Naples, Via P. Castellino 111, 80131 Napoli, Italy

[§]National Research Council, SPIN Institute, Unit of Salerno and Department of Physics "E. R. Caianiello", Università di Salerno, Via Ponte don Mellillo, 84084 Fisciano, Salerno, Italy

Supporting Information

ABSTRACT: A colorimetric immunosensor based on local surface plasmon resonance by gold nanoparticles is presented, and its application for the detection of human immunoglobulin G (IgG) is demonstrated. The color change of the colloidal solution is produced by nanoparticle aggregation, a process that can be tuned by the presence of the analyte once the nanoparticles are functionalized. In comparison to common functionalization techniques, the procedure described here is simpler, low-cost, and effective in binding antibodies upright on the gold surface. The dose−response curve is similar to that resulting in typical immunoassay platforms and is satisfactorily described by the proposed theoretical model. Human IgG at concentration levels of few hundreds of nanograms per milliliter can be detected by eyes within a few minutes, thereby making the colorimetric immunosensor proposed here a powerful tool in several areas, with urine test in medical diagnostics being the most immediate.

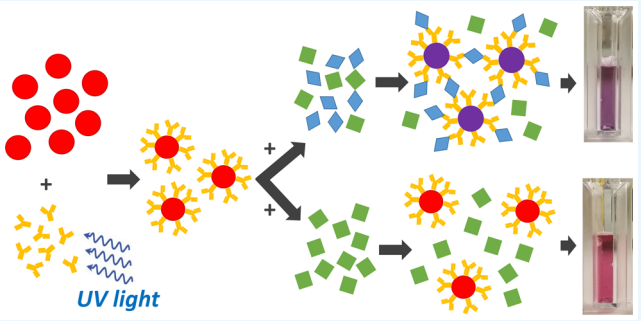

INTRODUCTION

Nanoparticle-based biosensors are often proposed due to their unique optical properties.[1,2] In recent years, considerable efforts have been directed to develop low-cost, easy, and rapid colorimetric diagnostics tools for point-of-care application or even for home use,[1] for example, for glucose monitoring.[3,4] The interaction of light with a metal nanoparticle may induce coherent and nonpropagating oscillations of free electrons with a resonance frequency, called localized surface plasmon resonance (LSPR).[5,6] The principal effects are the enhancement of the electromagnetic fields near the nanoparticle surface and the appearance of a strong extinction peak.[7] For gold and silver nanoparticles, the LSPR falls in the visible range, but gold is generally preferred due to its biocompatibility,[8] inertness,[9] and surface chemistry.[10] The LSPR depends on the local environment so that a change of the local refractive index leads to an LSPR spectral shift and also to a color variation of the colloidal solution.[11,12] For their capability of probing a nanoscale region around their surface, nanoparticles have been successfully employed in molecular sensing.[13−15] The colorimetric sensing based on gold nanoparticles (AuNPs) exploits the color change of the suspension from red to purple as a result of surface plasmon coupling between nanoparticles, until the transition from a dispersed to an aggregated state occurs.[16−19] AuNP aggregation can be tuned by using biological mechanisms, such as the antigen−antibody (Ab) interaction.[20] To induce AuNP aggregation only in the presence of the antigen, various strategies have been developed to immobilize properly oriented antibodies (Abs) on the AuNP surface.[21,22] The most used immobilization methods for Abs are based on the decoration of the AuNP surface with bifunctional or mediator linkers, which often require long chemical procedures;[23−25] moreover, AuNPs suffer from irreversible aggregation during functionalization with thiolate ligands.[26]

Alternative strategies to Abs for detecting proteins through the color change of a colloidal solution of AuNPs include the Lac-PEGylation of the gold surface for detecting *Ricinus communis* agglutinin,[27] aptamer−protein binding for the recognition of thrombin,[28] and lactose-stabilized AuNPs for the assessment of the presence of cholera toxin in stool.[29] Although the selectivity is satisfactory, all these methods for functionalizing gold surfaces share long and complex procedures that inherently lead to the lack of reproducibility.

Received: February 13, 2018
Accepted: March 26, 2018
Published: April 4, 2018

DOI: 10.1021/acsomega.8b00265
ACS Omega 2018, 3, 3805−3812

Recently, we have shown that Abs can be directly immobilized on gold surfaces by using a UV light-induced approach, known as photochemical immobilization technique (PIT).[30,31] Briefly, the absorption of UV light by nearby aromatic amino acids leads to the breakage of selected disulfide bridges, and the subsequent reactive thiol groups bind the gold substrate, providing strong anchoring sites. The effectiveness of PIT has been already demonstrated in several applications to the gold surface functionalization of quartz crystal microbalances.[32−35]

In this paper, we show that PIT is effective also with AuNPs, turning them into immunoprobes that aggregate in the presence of antigens. The whole process is depicted in Figure 1, where the first step is AuNP functionalization by means of

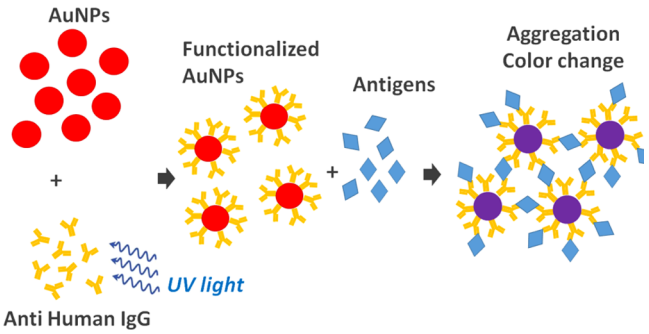

Figure 1. Detection scheme. The Abs are strongly anchored upright to AuNPs as a result of PIT. Because of the presence of multiple binding sites, the antigens act like linkers and clustering takes place.

UV-activated polyclonal antihuman immunoglobulin G (IgG), and the aggregation ensues from the multiple binding sites (epitopes) the antigens exhibit. Because polyclonal Abs and the presence of multiple binding sites on the antigens are the main conditions for clustering,[36] the antigens are symbolized by diamonds to highlight the generality of the scheme in Figure 1, which is expected to work also with other proteins. In this respect, although designed for the detection of IgG, the colorimetric immunoassay and most of the results described in the following are extendable to other targets.

RESULTS AND DISCUSSION

The synthesized AuNPs have been characterized by several techniques, the first of which is absorption spectroscopy (Figure S1), whereas the scanning electron microscope (SEM) images are reported in Figure 2a, which highlights the presence of quite regular spherical monodisperse nanoparticles with a diameter of approximately 40 nm. Figure 2b shows the UV−vis absorption spectra of the same AuNPs (solid black line) that reveal an LSPR band centered at 530.2 nm, as expected for spherical AuNPs with 40 nm.[37] Dynamic light scattering (DLS) measurements confirmed the AuNP size, providing a hydrodynamic diameter of about 40 nm and a polydispersity index of 0.2 (Figure S2). The contribution to the intensity at small hydrodynamics radii comes from the presence of the seeds formed during nanoparticle synthesis. Nevertheless, the aggregation process reported in Figure 3 suggests a negligible role played by these impurities in the whole procedure. The mean ζ potential has been measured to be -32 ± 1 mV, thereby confirming the existence of electrostatic repulsion forces among the particles that prevent their aggregation (Figure S3).

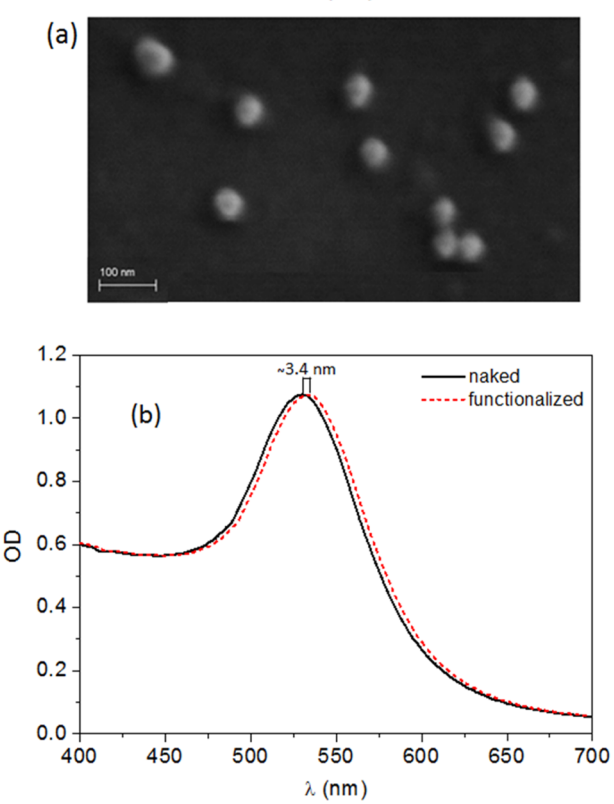

Figure 2. (a) SEM image of the synthesized AuNPs. (b) UV−vis absorption spectra of naked nanoparticles (solid black line) and the same after AuNPs have been functionalized with anti-IgG (dashed red line).

After the functionalization with IgG, the solution is centrifuged and the AuNPs, which constitute the pellet, are resuspended in pure water. The dotted red line in Figure 2b shows that the functionalized nanoparticles have the same spectrum only red-shifted by $\Delta\lambda \sim 3.4$ nm (dotted red line) as a consequence of the protein layer tethered to the gold surface. The two spectra show the same overall shape and intensity, thereby demonstrating a successful conjugation of the antibody to the gold surface, which leads to no lack of AuNP during the centrifugation and the subsequent change of the solvent.

Because the value of $\Delta\lambda$ can be related to the thickness of the protein layer, the effectiveness of PIT as a functionalization technique for AuNP can be further checked by estimating the average number each nanoparticle binds. Following the discussion reported by Pollitt et al.,[38] we set d as the nanoparticle (gold) core diameter and s as the dielectric coating thickness so that the fraction, g, of the total nanoparticle that is the shell is achieved by a simple geometrical consideration, that is

$$\frac{(d/2)^3}{(d/2+s)^3} + g = 1 \quad (1)$$

In the Rayleigh approximation, the shift of the resonance peak is[38]

$$\Delta\lambda = \frac{\lambda_p^2(\varepsilon_s - \varepsilon_m)g}{\lambda_{max,0}[1 + 2\alpha_s(1-g)]} \quad (2)$$

where λ_p is the free electron oscillation wavelength (131 nm for gold), $\lambda_{max,0}$ is the wavelength of maximum absorption for

DOI: 10.1021/acsomega.8b00265
ACS Omega 2018, 3, 3805−3812

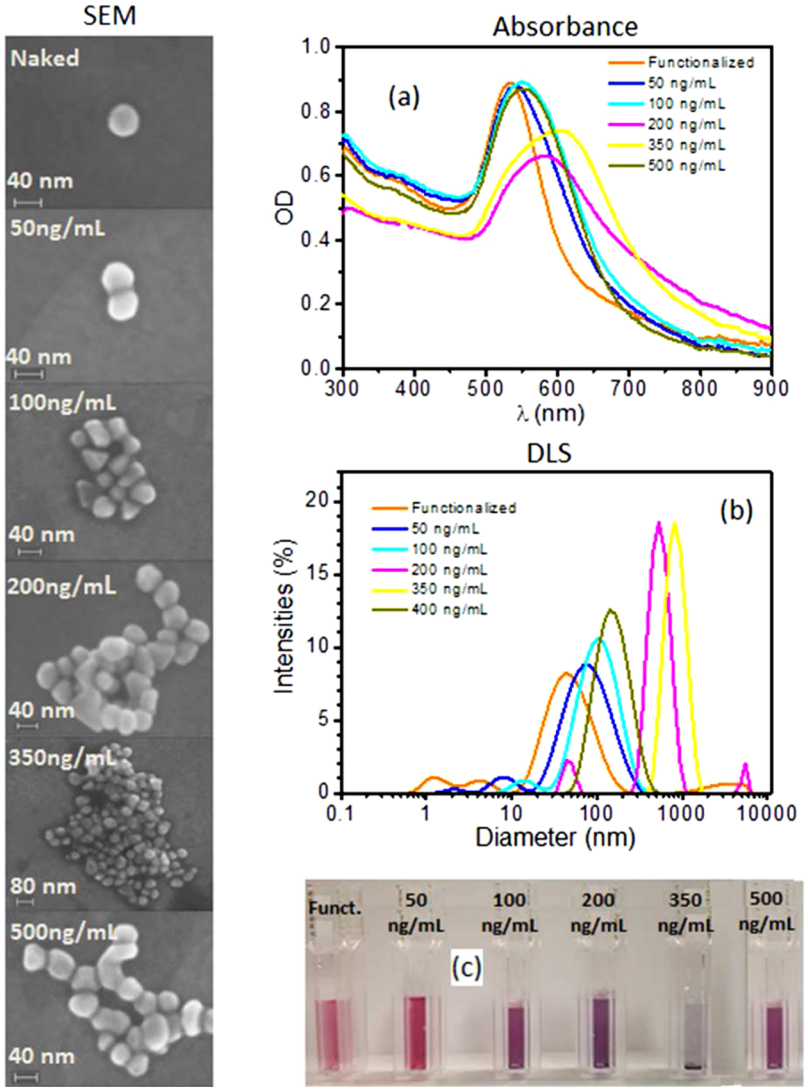

Figure 3. Left panel: SEM images of clusters in solution as a function of human IgG. The trend of increasing size is clear until a maximum is achieved at approximately 350 ng/mL. The subsequent increase to 500 ng/mL prevents AuNPs from forming larger clusters, and the hook effect takes place, making the cluster size at 500 ng/mL smaller than that obtained at 350 ng/mL. Right panel: (a) absorption spectra measured at several human IgG concentrations. The absorption peak is red-shifted as the concentration increases until a maximum is reached at 350 ng/mL. At the higher concentration of 500 ng/mL, the peak is shifted toward lower wavelength. (b) Hydrodynamic diameter measured by DLS shows the same hook effect reported for the absorption as well as for the cluster size. (c) Color change induced by particle aggregation. The layer on the bottom of the cuvette observed at 350 ng/mL is due to the precipitation caused by the large size of the clusters. This picture was taken after overnight storage.

uncoated colloids (530.2 nm for our AuNPs), ε is the relative permittivity (the subscripts s and m refer to the shell and the surrounding medium, respectively), and $\alpha_s = (\varepsilon_s - \varepsilon_m)/(\varepsilon_s + 2\varepsilon_m)$ is the polarizability of a sphere of shell dielectric constant, ε_s (2.02 by assuming the refraction index n_s = 1.42 for the protein[39]), in a medium of dielectric constant, ε_m (1.77 by assuming the refraction index n_m = 1.33 for the water). By inverting eq 2, we get g = 0.43, which in turn provides $s \sim 4$ nm through eq 1.

In a wide range of concentrations, the refractive index is a linear function of the concentration[40] and, hence, the absolute amount of adsorbed protein, Γ, can be determined by the De Feijter formula[41]

$$\Gamma = s\frac{n_s - n_m}{\frac{dn}{dC}} \quad (3)$$

where dn/dC is the increment of the refractive index due to concentration increase, which assumes a typical value of 0.19 mL/g for protein.[42] Thus, eq 3 provides $\Gamma \sim 200$ ng/cm^2, which corresponds to approximately 40 Abs (Ab molecular weight approximately 150 kDa) around a sphere with d = 40 nm. It is worth observing that the mean area occupied by each antibody is approximately 10^{-12} cm^2 whose square root is 10 nm, which corresponds to the linear dimension of the Ab. This result is what one would expect if the AuNPs are fully covered by antibodies, which bind the gold surface as reported in our previous paper,[31] that is, with one Fab well exposed and the other Fab tethered to the surface together with Fc.

The formation of a protein corona around the AuNP surface entails an increase of the local refractive index, which leads to a red shift of the resonance peak position. It is worth noticing that the absorption spectrum of the functionalized AuNPs was recorded after only 5 min of incubation; although short, this time is more than enough to reach the equilibrium because no

DOI: 10.1021/acsomega.8b00265
ACS Omega 2018, 3, 3805−3812

change in the absorption spectrum was observed after 5 min (Figure S4). Furthermore, the LSPR peak position was unchanged after both the centrifugation and the blocking with bovine serum albumin (BSA) (Figure S5), suggesting the effectiveness of PIT in AuNPs because it provides both a stable attachment and a high surface coverage.

The behavior of AuNPs as a biosensor is described in Figure 3, where the left panel reports the change of cluster size induced by the antigens (human IgGs) that act as linkers between nanoparticles when grafted on their surface. The structures reported in the left panel are representative of the cluster size distributions, the latter being deducible by the SEM images at lower magnification, reported in Figure S6, for several antigen concentrations. As clearly observable in Figure 3, the presence of the analyte promotes aggregation until the optimum concentration of about 350 ng/mL is reached; after that, further increase of the concentration hampers the aggregation. This is because beyond such a value the AuNPs are saturated with the antigens, which do not bind each other, thereby preventing nanoparticles from aggregating. Such a dynamics is well-known in immunology as prozone or hook effect and may give rise to false negative when the analyte concentration is too high.[43] This undesirable effect can be easily overcome with a double measurement at two different concentrations (serial dilutions) so that one can easily discriminate whether the low signal arises from a concentration that is too low or too high.

The optical response of the solution in presence of the analyte is reported in the right panel of Figure 3 together with the characterization by DLS. In particular, Figure 3a shows the absorption spectra of the functionalized AuNPs at various concentrations of human IgG. The spectra are collected after an incubation of 15′, a time long enough to achieve a condition close to the equilibrium (see Figure S7). Both the LSPR peak position and width depend crucially on the amount of human IgG added to the functionalized AuNPs, thus evidencing the high sensitivity of the biosensor. The absorbance of the functionalized AuNPs is slightly lower than that reported in Figure 2 because of the different approach used in removing the supernatant after the centrifugation; in fact, for sensing purposes, it is necessary to get rid of the whole supernatant to remove all of the free Abs in the solution, and this operation unavoidably leads to the removal of some AuNps. The aggregates are further characterized by dynamic light scattering, and the intensity distributions of the particle sizes confirm the hook effect observed in the absorption spectra. The size of the cluster increases up to a maximum, which corresponds to a concentration of human IgG of 350 ng/mL; after that, it reduces (Figure 3b). Interestingly, the size measured by DLS is in good agreement with that obtained by SEM analysis reported in the left panel of Figure 3, ranging from 42 nm for the bare functionalized AuNPs to a maximum of approximately 800 nm measured when a solution of 350 ng/mL human IgG is mixed with AuNPs. The last SEM picture in the left panel of Figure 3 (bottom left) still confirms to a large extent the decrease of the dimensions of AuNPs clusters to 185 nm as measured by the DLS for larger values of human IgG concentration. Figure 3c reports a picture of the cuvettes that shows the change of the color induced by the analyte. In addition, in this case, the hook effect brings about a return of the color toward red when the human IgG concentration is larger than 350 ng/mL. At this concentration, the size of the cluster is so high that particle precipitation occurs, manifesting itself as a layer at the bottom of the fifth cuvette in Figure 3c.

By comparing the results presented in Figure 3a,b, we obtain the relation between the red shift and the dimension of the aggregate reported in Figure 4 (this figure also includes additional measurements not shown in Figure 3 for the sake of clarity). After a rapid increase, presumably corresponding to the formation of dimers, the shift grows roughly linearly with the dimension of the aggregates. The whole plot evidences the role played by the dipole−dipole interaction occurring in a nanoparticle aggregate. The quantitative description of such a process, which depends strongly on parameters such as the separation distance between the AuNPs and their diameter, requires numerical modeling, which goes beyond the scope of the present work. However, the optical properties of gold nanoparticle aggregates have been addressed in a number of papers, all of them reporting the occurrence of LSPR red-shift when more particles interact.[11,16,44−46] In particular, it has been shown that a cluster made of 13 AuNPs with a diameter equal to 40 nm and far apart by a distance that is 20% the diameter gives rise to a shift that is approximately 2% the wavelength of maximum absorption for uncoated AuNPs.[47] The SEM pictures shown in the left panel in Figure 3 are obviously taken in vacuum, and as such the Abs are dried and their size is underestimated. However, from eq 1, we estimated the thickness of the protein corona as $s \sim 4$ nm; thus, by neglecting the contribution of the linker, the separation distance in our clusters is ∼8 nm, which corresponds to 20% of the diameter. Moreover, the size of a cluster made of 13 AuNPs is approximately 150 nm (linear dimension). Strikingly, the plot shown in Figure 4 shows that such an aggregate provides approximately 10−15 nm red-shift, a value in excellent agreement with theory.[47]

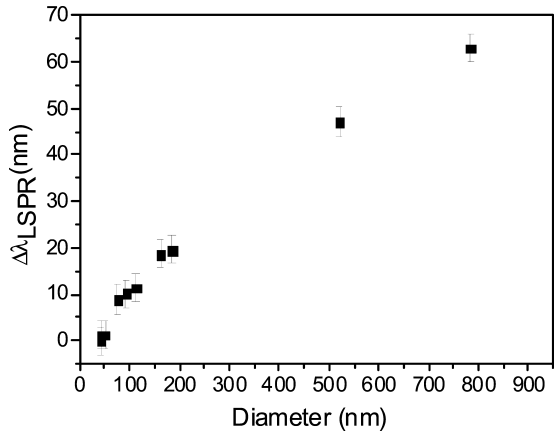

Figure 4. Shift of the wavelength of maximum absorption as a function of hydrodynamic diameter measured by the DLS.

The shift of the resonance peak wavelength as a function of human IgG concentration is reported in Figure 5, which constitutes the dose−response curve for the colorimetric immunosensor. At human IgG concentration lower than 20 ng/mL, only a small shift (<2 nm) of the resonance wavelength is observed, but at higher analyte concentrations, a significant red-shift occurs, which is responsible for the color change from red to purple visible in Figure 3c.

The peak in the dose−response signal and the region around it are referred to as hook point and zone of equivalence, respectively. At concentrations below the hook point, the

DOI: 10.1021/acsomega.8b00265
ACS Omega 2018, 3, 3805−3812

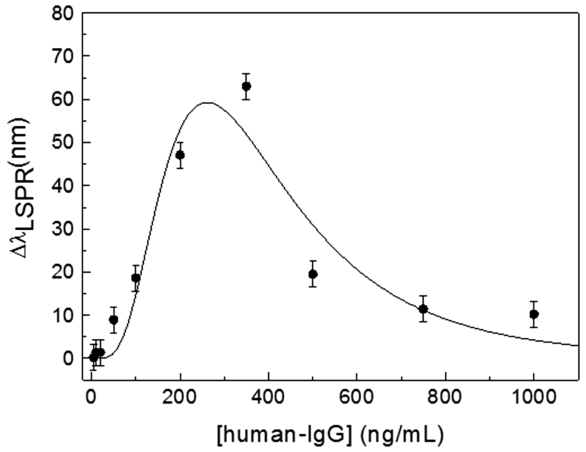

Figure 5. Shift of the wavelength of maximum absorption as a function of analyte concentration (human IgG). The curve is the best fit achieved with eq 5.

number of human IgG is relatively low and aggregation is not optimized (small red-shift), whereas at concentration of human IgG above the hook point, the binding sites of the AuNPs tend to saturate again, resulting in a reduced cross-linking and, hence, a small red-shift is observed again. Although aggregation dynamics is a complex process and its quantitative description would require sophisticated approaches of statistical mechanics, we are able to capture the underlying physics by considering a very simplified version of the system. Let us consider a colloidal solution made of two species: functionalized AuNPs that have bound the analyte and are therefore "saturated" (specie A) and those AuNPs available to bind the analyte (specie B). The concentrations [A] and [B] are linked by the relation [A] + [B] = $[AuNP]_0$, the right-hand side being the initial concentration of AuNP. At equilibrium, we have

$$[A] = \frac{[AuNP]_0[IgG]}{K + [IgG]} \tag{4}$$

and

$$[B] = [AuNP]_0 - [A] = [AuNP]_0 \frac{K}{K + [IgG]} \tag{5}$$

where K is the equilibrium constant of the reaction B + IgG → A. Thus, the role played by the analyte (IgG) is to shift the equilibrium between [A] and [B]: the larger the [IgG], the smaller the [A] and, in turn, the larger the [B]. The aggregation is a multiple-order complexation between A and B, and its optical response depends almost linearly on its size (see Figure 4). Thus, we expect that the optical response will follow a power law in its dependence on the product [A][B], that is

$$\Delta\lambda = \left(\frac{R[IgG]}{(K + [IgG])^2}\right)^n \tag{6}$$

where R includes both the nanoparticle concentration and the instrument response.

The best fit of the experimental data with eq 6 provides R^n = $(2000 \pm 300)^n$ nm $(ng/mL)^n$, K = 260 ± 20 ng/mL, and n = 6.3 ± 1.6 and is reported as a solid line in Figure 5. The agreement with the experimental data is more than satisfactory and shows that eq 5, though simple, is able to capture the essence of a complex process that includes aggregation of gold nanoparticles and their response to the electromagnetic field.

By taking three times the standard deviation (±3 nm), a limit of detection <100 ng/mL (700 pM) can be inferred from the dose−response curve, whereas the range of the positive response is 50−500 ng/mL. Although this range is of interest in a number of applications,[48] in medical diagnostics the IgG concentration can be much higher, reaching the value of hundreds of micrograms per milliliter. This issue is addressed by carrying out serial dilution of the sample, a procedure that is customary in immunoassay.[49] The drawback of this procedure is the unfeasibility of the one-step measurement, but the cost effectiveness of our system, along with ease of use as well as prompt response, softens this drawback, making the proposed immunosensor a suitable platform for mass screening. Moreover, it has to be considered that the aggregation process can be optimized by properly designing the protein corona,[36] whereas the range of positive response of the immunoassay can be tuned to a large extent by adjusting the concentration of AuNP probes.[50]

To evaluate the specificity of the immunosensor, we checked possible cross-reactions with a similar protein, that is, the mouse IgG, which is comparable to the Fc unit. To this end, 4 μL of a solution containing 50 μg/mL mouse IgG was added to 1 mL of the sensing solution containing approximately 6×10^{10} AuNPs/mL (see the Materials and Methods). The absorption spectra measured after 1 and 24 h incubation showed no change (see Figure S8), thereby demonstrating not only the lack of any cross-reaction with mouse IgG, but also the long-term stability of the functionalized colloidal solution.

CONCLUSIONS

In this work, we described a colorimetric immunosensor for the detection of human IgG based on Ab-functionalized gold nanoparticles. The specificity is inherently warranted by the presence of antibodies acting as recognition biomolecules, whereas the performances in terms of sensitivity and limit of detection allow its application in a number of circumstances where fast response is required, even if it is of "on−off" type. The stability of the colloidal solution is noticeable thanks to the photochemical immobilization technique we have adopted for the functionalization. The presence of human IgG is visualized as a change of the color the solution undergoes due to the formation of aggregates. Such a process is very similar to that occurring in the agglutination tests and has been analyzed by a simple theoretical model that captures the main features of the dose−response curve, particularly the prozone effect. The possible artifacts brought about by this effect can be easily overcome by serial dilutions made affordable by the prompt response (few minutes) and ease of use shown by the immunosensor proposed here. The positive response range for IgG is 50−500 ng/mL, thereby making it suitable for application to medical diagnostic in a number of circumstances, for instance, for detecting proteinuria, a pathological condition in which IgG concentration reaches values much larger than 1 mg/mL.[51] Such a concentration can be easily detected by our immunosensor with 1:1000 dilution (or more), which would fully preserve the solvent characteristics and the nanoparticle stability. The application of the whole procedure to other analytes, but even the study of the role played by the diameter of the nanoparticles in the aggregation process, will be the next steps of this research.

DOI: 10.1021/acsomega.8b00265
ACS Omega 2018, 3, 3805−3812

MATERIALS AND METHODS

Materials. Gold(III) chloride trihydrate ($HAuCl_4{\cdot}3H_2O$), sodium citrate, and bovine serum albumin (BSA) were purchased from Sigma-Aldrich. Goat antihuman IgG, human IgG, and IgG from mouse were obtained from ImmunoReagents, Inc. Ultrapure water from Milli-Q system was used for all preparations.

Synthesis of AuNPs. Spherical gold nanoparticles were synthesized by modifying an already-existing protocol.[38] A gold salt solution composed of 50 mL of ultrapure water and 500 μL and 8 mg/mL of $HAuCl_4{\cdot}3H_2O$ was prepared and boiled under constant stirring. Thus, 6 mL of 10 mg/mL sodium citrate was added, and the resulting solution was boiled for 2 min to achieve particles nucleation. After that, 4.8 mL of 8 mg/mL $HAuCl_4{\cdot}3H_2O$ was added to induce particles growth, and the stirring of the boiling solution was continued for 2 min. At the end of this process, the color of the suspension turned dark red, with the absorption spectrum shown in Figure S1, from which the optical density of approximately 0.6 at 450 nm allowed us to estimate the AuNP concentration as 6×10^{10} AuNPs/mL.[52] Afterward, the AuNPs colloid was stored in the dark at 4 °C.

PIT-Functionalization of AuNPs. To remove impurities present in the stock solution, 1 mL of AuNPs was centrifuged at 3000 g for 10 min; then, the supernatant was discarded and the AuNP pellet was resuspended in ultrapure water. A solution of 50 μg/mL antihuman IgG was prepared and irradiated for 1 min with a HERAEUS amalgam-type NNI 40/20 lamp emitting at 254 nm with a power of 40 W. The lamp is approximately 20 cm long and has a diameter of 1 cm so that the intensity is about 0.7 W/cm^2, very close to the surface. By considering that the cuvette containing the antihuman IgG solution is located at 1 cm from the lamp surface, the effective irradiation intensity used for the antibody activation is about 0.3 W/cm^2. A volume of 20 μL of the irradiated antihuman IgG solution was added to 1 mL of AuNPs, and the resulting mixture was incubated for 3 min. The amount of antihuman IgG present in the mixture was progressively increased by adding 4 μL of the irradiated antibody solution. The UV−vis absorption spectra showed red shift of the maximum absorption wavelength as a result of the formation of the protein corona. Only few spikes were necessary to stabilize the red shift; thus, a total number of five additions, corresponding to 1 μg/mL antihuman IgG concentration, were chosen to ensure the maximum coverage of the AuNP surfaces. The unbound antibodies were removed from the mixture by centrifugation at 3000 g for 10 min, and the antihuman IgG functionalized AuNP pellet was resuspended in ultrapure water. After that, 1 mg/mL BSA was added to the functionalized colloid to block the AuNP surface from nonspecific adsorption.

Colorimetric Immunoassay. Various amounts of human IgG in the range of 5 ng/mL to 1 μg/mL were added to 1 mL of aliquots of the antihuman IgG functionalized AuNPs, and the samples were incubated at room temperature. Then, UV−vis absorption spectra from 400 to 700 nm were collected at different incubation times to study the optical response of the system and how it changed in time.

Instruments. UV−vis absorption spectroscopy and dynamic light scattering (DLS) were used here to characterize both bare and antihuman IgG functionalized AuNPs and to study the optical response of the functionalized colloid in presence of the antigen human IgG. The UV−vis absorption spectra were recorded on a Jenway 6715 UV/vis spectrophotometer with 0.1 nm resolution and 0.2 nm spectral bandwidth. DLS measurements were conducted using a Zetasizer Nano ZS (Malvern Instruments) equipped with a 633 nm He−Ne laser and an avalanche photodiode detector placed at the detection angle of 173°. The same instrument was able to perform ζ-potential measurements based on laser Doppler microelectrophoresis.

The morphology of the synthesized AuNPs was analyzed by a Zeiss ∑IGMA field emission scanning electron microscope (FESEM) with a nominal resolution of ∼3 nm at 1 kV. SEM images of the sample surface have been registered by recording secondary electrons (SEs) using both an Everhart-Thornley and an In-Lens (IL) detector. The IL detector, located inside the electron column of the microscope and arranged rotationally symmetric around its axis, allows the collection of SE with high efficiency. Therefore, the IL detector provides SEM images with higher contrast that are used to obtain zoomed views of sample portions with higher magnification. FESEM has also been used to image the clusters made of the antihuman IgG functionalized AuNPs induced by the human IgG.

ASSOCIATED CONTENT

Supporting Information

The Supporting Information is available free of charge on the ACS Publications website at DOI: 10.1021/acsomega.8b00265.

Characterization of AuNPs by UV−vis absorption spectroscopy, DLS, and ζ-potential measurements (Figures S1−S3); UV−vis spectra of AuNP colloidal solutions that show the need of very short incubation time for functionalization (Figure S4); the strength of the bond between Abs and AuNPs (Figure S5); larger area images from SEM microscopy (Figure S6); response time of the immunosensor (Figure S7); and the specificity/stability test (Figure S8) (PDF)

AUTHOR INFORMATION

Corresponding Author

*E-mail: rvelotta@unina.it.

ORCID

Raffaele Velotta: 0000-0003-1077-8353

Present Address

‖Italian Institute of Technology, Via Morego 30, 16163 Genova, Italy (M.I.).

Notes

The authors declare no competing financial interest.

ACKNOWLEDGMENTS

R.V. and B.D.V. acknowledge the financial support of "Fondazione con il Sud" (Project No. 2011-PDR-18, "Biosensori piezo elettrici a risposta in tempo reale per applicazioni ambientali e agro-alimentari").

ABBREVIATIONS

LSPR, localized surface plasmon resonance; AuNP, gold nanoparticle; PIT, photochemical immobilization technique; Ab, antibody; IgG, immunoglobulin; DLS, differential light scattering; SEM, scanning electron microscope

REFERENCES

(1) Tang, L.; Li, J. Plasmon-Based Colorimetric Nanosensors for Ultrasensitive Molecular Diagnostics. *ACS Sens.* **2017**, *2*, 857−875.

DOI: 10.1021/acsomega.8b00265
ACS Omega 2018, 3, 3805−3812

(2) Zhang, Y.; Guo, Y.; Xianyu, Y.; Chen, W.; Zhao, Y.; Jiang, X. Nanomaterials for Ultrasensitive Protein Detection. *Adv. Mater.* **2013**, *25*, 3802−3819.
(3) Liu, Q.; Yang, Y.; Li, H.; Zhu, R.; Shao, Q.; Yang, S.; Xu, J. NiO Nanoparticles Modified with 5,10,15,20-tetrakis(4-Carboxyl Pheyl)-Porphyrin: Promising Peroxidase Mimetics for H_2O_2 and Glucose Detection. *Biosens. Bioelectron.* **2015**, *64*, 147−153.
(4) Zhu, X.; Chen, W.; Wu, K.; Li, H.; Fu, M.; Liu, Q.; Zhang, X. A Colorimetric Sensor of H_2O_2 Based on Co_3O_4−montmorillonite Nanocomposites with Peroxidase Activity. *New J. Chem.* **2018**, *42*, 1501−1509.
(5) Li, M.; Cushing, S. K.; Wu, N. Plasmon-Enhanced Optical Sensors: A Review. *Analyst* **2015**, *140*, 386−406.
(6) Chen, Y.; Ming, H. Review of Surface Plasmon Resonance and Localized Surface Plasmon Resonance Sensor. *Photonic Sens.* **2012**, *2*, 37−49.
(7) Petryayeva, E.; Krull, U. J. Localized Surface Plasmon Resonance: Nanostructures, Bioassays and Biosensing—A Review. *Anal. Chim. Acta* **2011**, *706*, 8−24.
(8) Shukla, R.; Bansal, V.; Chaudhary, M.; Basu, A.; Bhonde, R. R.; Sastry, M. Biocompatibility of Gold Nanoparticles and Their Endocytotic Fate inside the Cellular Compartment: A Microscopic Overview. *Langmuir* **2005**, *21*, 10644−10654.
(9) Zhang, X. Gold Nanoparticles: Recent Advances in the Biomedical Applications. *Cell Biochem. Biophys.* **2015**, *72*, 771−775.
(10) Chaudhary, A.; Khan, S.; Gupta, A.; Nandi, C. K. Effect of Surface Chemistry and Morphology of Gold Nanoparticle on the Structure and Activity of Common Blood Proteins. *New J. Chem.* **2016**, *40*, 4879−4883.
(11) Amendola, V.; Pilot, R.; Frasconi, M.; Maragò, O. M.; Iatì, M. A. Surface Plasmon Resonance in Gold Nanoparticles: A Review. *J. Phys.: Condens. Matter* **2017**, *29*, No. 203002.
(12) Mock, J. J.; Smith, D. R.; Schultz, S. Local Refractive Index Dependence of Plasmon Resonance Spectra from Individual Nanoparticles. *Nano Lett.* **2003**, *3*, 485−491.
(13) Lee, K.-S.; El-Sayed, M. A. Gold and Silver Nanoparticles in Sensing and Imaging: Sensitivity of Plasmon Response to Size, Shape, and Metal Composition. *J. Phys. Chem. B* **2006**, *110*, 19220−19225.
(14) Mayer, K. M.; Hafner, J. H. Localized Surface Plasmon Resonance Sensors. *Chem. Rev.* **2011**, *111*, 3828−3857.
(15) Khashab, N. M.; Durand, J.-O.; Zink, J. I. Engineering Nanoparticles for Sensing and Biomedical Applications: A Themed Collection. *Mol. Syst. Des. Eng* **2017**, *2* (4), 347−348.
(16) Ghosh, S. K.; Pal, T. Interparticle Coupling Effect on the Surface Plasmon Resonance of Gold Nanoparticles: From Theory to Applications. *Chem. Rev.* **2007**, *107*, 4797−4862.
(17) Politi, J.; Spadavecchia, J.; Iodice, M.; de Stefano, L. Oligopeptide−Heavy Metal Interaction Monitoring by Hybrid Gold Nanoparticle Based Assay. *Analyst* **2015**, *140*, 149−155.
(18) Politi, J.; De Stefano, L.; Rea, I.; Gravagnuolo, A. M.; Giardina, P.; Methivier, C.; Casale, S.; Spadavecchia, J. One-Pot Synthesis of a Gold nanoparticle−Vmh2 Hydrophobin Nanobiocomplex for Glucose Monitoring. *Nanotechnology* **2016**, *27*, No. 195701.
(19) Nilam, M.; Hennig, A.; Nau, W. M.; Assaf, K. I. Gold Nanoparticle Aggregation Enables Colorimetric Sensing Assays for Enzymatic Decarboxylation. *Anal. Methods* **2017**, *9*, 2784−2787.
(20) Lesniewski, A.; Los, M.; Jonsson-NiedzioÌåka, M.; Krajewska, A.; Szot, K.; Los, J. M.; Niedziolka-Jonsson, J. Antibody Modified Gold Nanoparticles for Fast and Selective, Colorimetric T7 Bacteriophage Detection. *Bioconjugate Chem.* **2014**, *25*, 644−648.
(21) Tiwari, P. M.; Vig, K.; Dennis, V. A.; Singh, S. R. Functionalized Gold Nanoparticles and Their Biomedical Applications. *Nanomaterials* **2011**, *1*, 31−63.
(22) Arruebo, M.; Valladares, M.; González-Fernández, Á. Antibody-Conjugated Nanoparticles for Biomedical Applications. *J. Nanomater.* **2009**, *2009*, 1−24.
(23) Liu, Y.; Zhang, L.; Wei, W.; Zhao, H.; Zhou, Z.; Zhang, Y.; Liu, S. Colorimetric Detection of Influenza A Virus Using Antibody-Functionalized Gold Nanoparticles. *Analyst* **2015**, *140*, 3989−3995.
(24) Jazayeri, M. H.; Amani, H.; Pourfatollah, A. A.; Pazoki-Toroudi, H.; Sedighimoghaddam, B. Various Methods of Gold Nanoparticles (GNPs) Conjugation to Antibodies. *Sens. Bio-Sens. Res.* **2016**, *9*, 17−22.
(25) Mustafaoglu, N.; Kiziltepe, T.; Bilgicer, B. Site-Specific Conjugation of an Antibody on a Gold Nanoparticle Surface for One-Step Diagnosis of Prostate Specific Antigen with Dynamic Light Scattering. *Nanoscale* **2017**, *9*, 8684−8694.
(26) Yeh, Y.-C.; Creran, B.; Rotello, V. M. Gold Nanoparticles: Preparation, Properties, and Applications in Bionanotechnology. *Nanoscale* **2012**, *4*, 1871−1880.
(27) Otsuka, H.; Akiyama, Y.; Nagasaki, Y.; Kataoka, K. Quantitative and Reversible Lectin-Induced Association of Gold Nanoparticles Modified with α-Lactosyl-ω-Mercapto-Poly(ethylene Glycol). *J. Am. Chem. Soc.* **2001**, *123*, 8226−8230.
(28) Pavlov, V.; Xiao, Y.; Shlyahovsky, B.; Willner, I. Aptamer-Functionalized Au Nanoparticles for the Amplified Optical Detection of Thrombin. *J. Am. Chem. Soc.* **2004**, *126*, 11768−11769.
(29) Schofield, C. L.; Field, R. A.; Russell, D. A. Glyconanoparticles for the Colorimetric Detection of Cholera Toxin. *Anal. Chem.* **2007**, *79*, 1356−1361.
(30) Ventura, B. D.; Schiavo, L.; Altucci, C.; Esposito, R.; Velotta, R. Light Assisted Antibody Immobilization for Bio-Sensing. *Biomed. Opt. Express* **2011**, *2*, No. 3223.
(31) Funari, R.; Ventura, B. D.; Altucci, C.; Offenhäusser, A.; Mayer, D.; Velotta, R. Single Molecule Characterization of UV-Activated Antibodies on Gold by Atomic Force Microscopy. *Langmuir* **2016**, *32*, 8084−8091.
(32) Funari, R.; Ventura, B. D.; Schiavo, L.; Esposito, R.; Altucci, C.; Velotta, R. Detection of Parathion Pesticide by Quartz Crystal Microbalance Functionalized with UV-Activated Antibodies. *Anal. Chem.* **2013**, *85*, 6392−6397.
(33) Funari, R.; Ventura, B. D.; Carrieri, R.; Morra, L.; Lahoz, E.; Gesuele, F.; Altucci, C.; Velotta, R. Detection of Parathion and Patulin by Quartz-Crystal Microbalance Functionalized by the Photonics Immobilization Technique. *Biosens. Bioelectron.* **2015**, *67*, 224−229.
(34) Ventura, B. D.; Sakač, N.; Funari, R.; Velotta, R. Flexible Immunosensor for the Detection of Salivary α-Amylase in Body Fluids. *Talanta* **2017**, *174*, 52−58.
(35) Ventura, B. D.; Iannaccone, M.; Funari, R.; Ciamarra, M. P.; Altucci, C.; Capparelli, R.; Roperto, S.; Velotta, R. Effective Antibodies Immobilization and Functionalized Nanoparticles in a Quartz-Crystal Microbalance-Based Immunosensor for the Detection of Parathion. *PLoS One* **2017**, *12*, No. e0171754.
(36) Yeo, E. L. L.; Chua, A. J. S.; Parthasarathy, K.; Yeo, H. Y.; Ng, M. L.; Kah, J. C. Y. Understanding Aggregation-Based Assays: Nature of Protein Corona and Number of Epitopes on Antigen Matters. *RSC Adv.* **2015**, *5*, 14982−14993.
(37) Njoki, P. N.; Lim, I.-I. S.; Mott, D.; Park, H.-Y.; Khan, B.; Mishra, S.; Sujakumar, R.; Luo, J.; Zhong, C.-J. Size Correlation of Optical and Spectroscopic Properties for Gold Nanoparticles. *J. Phys. Chem. C* **2007**, *111*, 14664−14669.
(38) Pollitt, M. J.; Buckton, G.; Piper, R.; Brocchini, S. Measuring Antibody Coatings on Gold Nanoparticles by Optical Spectroscopy. *RSC Adv.* **2015**, *5*, 24521−24527.
(39) Bell, N. C.; Minelli, C.; Shard, A. G. Quantitation of IgG Protein Adsorption to Gold Nanoparticles Using Particle Size Measurement. *Anal. Methods* **2013**, *5*, 4591.
(40) Vörös, J. The Density and Refractive Index of Adsorbing Protein Layers. *Biophys. J.* **2004**, *87*, 553−561.
(41) De Feijter, J. A.; Benjamins, J.; Veer, F. A. Ellipsometry as a Tool to Study the Adsorption Behavior of Syntetic and Biopolyers at the Air−Water Interface. *Biopolymers* **1978**, *17*, 1759−1772.
(42) Zhao, H.; Brown, P. H.; Schuck, P. On the Distribution of Protein Refractive Index Increments. *Biophys. J.* **2011**, *100*, 2309−2317.
(43) Fernando, S. A.; Wilson, G. S. Studies of the "hook" Effect in the One-Step Sandwich Immunoassay. *J. Immunol. Methods* **1992**, *151*, 47−66.

DOI: 10.1021/acsomega.8b00265
ACS Omega 2018, 3, 3805−3812

(44) Aili, D.; Selegård, R.; Baltzer, L.; Enander, K.; Liedberg, B. Colorimetric Protein Sensing by Controlled Assembly of Gold Nanoparticles Functionalized with Synthetic Receptors. *Small* **2009**, *5*, 2445−2452.
(45) Chegel, V.; Rachkov, O.; Lopatynskyi, A.; Ishihara, S.; Yanchuk, I.; Nemoto, Y.; Hill, J. P.; Ariga, K. Gold Nanoparticles Aggregation: Drastic Effect of Cooperative Functionalities in a Single Molecular Conjugate. *J. Phys. Chem. C* **2012**, *116*, 2683−2690.
(46) Jans, H.; Huo, Q. Gold Nanoparticle-Enabled Biological and Chemical Detection and Analysis. *Chem. Soc. Rev.* **2012**, *41*, 2849−2866.
(47) Zámbó, D.; Deák, A. Optical Simulations of Self-Assembly Relevant Gold Aggregates: A Comparative Study. *Period. Polytech., Chem. Eng.* **2016**, *60*, 244−251.
(48) Brangel, P.; Sobarzo, A.; Parolo, C.; Miller, B. S.; Howes, P. D.; Gelkop, S.; Lutwama, J. J.; Dye, J. M.; McKendry, R. A.; Lobel, L.; et al. A Serological Point-of-Care Test for the Detection of IgG Antibodies against Ebola Virus in Human Survivors. *ACS Nano* **2018**, 63.
(49) Dasgupta, A.; Wahed, A. Immunoassay Platform and Designs. In *Clinical Chemistry, Immunology and Laboratory Quality Control*; Elsevier, 2014; pp 19−34.
(50) Driskell, J. D.; Jones, C. A.; Tompkins, S. M.; Tripp, R. A. One-Step Assay for Detecting Influenza Virus Using Dynamic Light Scattering and Gold Nanoparticles. *Analyst* **2011**, *136*, 3083.
(51) Khamis, R. Y.; Hughes, A. D.; Caga-Anan, M.; Chang, C. L.; Boyle, J. J.; Kojima, C.; Welsh, P.; Sattar, N.; Johns, M.; Sever, P.; et al. High Serum Immunoglobulin G and M Levels Predict Freedom From Adverse Cardiovascular Events in Hypertension: A Nested Case-Control Substudy of the Anglo-Scandinavian Cardiac Outcomes Trial. *EBioMedicine* **2016**, *9*, 372−380.
(52) Haiss, W.; Thanh, N. T. K.; Aveyard, J.; Fernig, D. G. Determination of Size and Concentration of Gold Nanoparticles from UV−Vis Spectra. *Anal. Chem.* **2007**, *79*, 4215−4221.

DOI: 10.1021/acsomega.8b00265
ACS Omega 2018, 3, 3805−3812